Electromagnetic transition rates in the $N = 80$ nucleus $^{138}_{58}$Ce

T. Alharbi,[1,2] P. H. Regan,[1] P. J. R. Mason,[1] N. Mărginean,[3] Zs. Podolyák,[1] A. M. Bruce,[4] E. C. Simpson,[1] A. Algora,[5] N. Alazemi,[1] R. Britton,[1] M. R. Bunce,[1] D. Bucurescu,[3] N. Cooper,[6] D. Deleanu,[3] D. Filipescu,[3] W. Gelletly,[1] D. Ghiță,[3] T. Glodariu,[3] G. Ilie,[3,6] S. Kisyov,[7] J. Lintott,[1] S. Lalkovski,[7] S. Liddick,[8] C. Mihai,[3] K. Mulholland,[9] R. Mărginean,[3] A. Negret,[3] M. Nakhostin,[1] C. R. Nita,[3] O. J. Roberts,[4] S. Rice,[1] J. F. Smith,[9] L. Stroe,[3] T. Sava,[3] C. Townsley,[1] E. Wilson,[1] V. Werner,[6] M. Zhekova,[7] and N. V. Zamfir[3]

[1]*Department of Physics, University of Surrey, Guildford, GU2 7XH, UK*
[2]*Department of Physics, Almajmaah University, P.O. Box 66, 11952, Saudi Arabia*
[3]*Horia Hulubei - National Institute for Physics and Nuclear Engineering (IFIN-HH), Bucharest, Romania*
[4]*School of Computing Engineering and Mathematics, University of Brighton, Brighton, BN2 4GJ, UK*
[5]*IFIC, CSIC-Universidad de Valencia, A.C. 22085, E 46071, Valencia, Spain*
[6]*Wright Nuclear Structure Laboratory, Yale University, New Haven, Connecticut 06520-8120, USA*
[7]*Faculty of Physics, University of Sofia St. Kliment Ohridski, BG-1164 Sofia, Bulgaria*
[8]*National Superconducting Cyclotron Laboratory (NSCL), Michigan State University, East Lansing, Michigan 48824, USA*
[9]*School of Engineering, University of the West of Scotland, High Street, Paisley PA1 2BE, UK*

(Received 15 November 2012; revised manuscript received 12 December 2012; published 17 January 2013)

The half-life of the $I^\pi = 6^+$ yrast state at $E_x = 2294$ keV in ^{138}Ce has been measured as $T_{1/2} = 880(19)$ ps using the fast-timing γ-ray coincidence method with a mixed $LaBr_3$(Ce)-HPGe array. The excited states in ^{138}Ce have been populated by the ^{130}Te(^{12}C, $4n$) fusion-evaporation reaction at an incident beam energy of 56 MeV. The extracted $B(E2; 6_1^+ \rightarrow 4_1^+) = 0.101(24)$ W.u. value is compared with the predictions of truncated basis shell model calculations and with the systematics of the region. This shows an anomalous behavior compared to the neighboring isotonic and isotopic chains. Half-lives for the yrast 5^-, 11^+ and 14^+ states in ^{138}Ce have also been determined in this work.

DOI: 10.1103/PhysRevC.87.014323 PACS number(s): 21.10.Tg, 23.20.Lv, 27.60.+j

I. INTRODUCTION

Electromagnetic transition rates in nuclei in the vicinity of closed shells can be used as a precision test of the restricted basis shell model and also provide information on the effective charges used as inputs to such calculations. The $N = 80$ isotonic chain allows a consistent test of shell model predictions for proton numbers above the $Z = 50$ shell closure where the near-yrast states in such nuclei can be associated largely with configurations of well-defined proton-particle/neutron-hole make up. The $N = 80$ isotonic chain exhibits yrast $I^\pi = 10^+$ isomeric states in all its even-Z members from $^{130}_{50}$Sn up to $^{148}_{68}$Er [1–6], with this structure in the lighter isotones being associated with a predominantly $\nu(h_{11/2})^{-2}_{10^+}$ maximally aligned configuration. In the case of the $Z = 56$ [7] system, ^{136}Ba, the lower lying yrast states have been characterized by either negative parity states from neutron $(h_{11/2} \otimes d_{3/2})$ or $(h_{11/2} \otimes s_{1/2})$ configurations or positive parity from proton $(d_{5/2})^2$, $(g_{7/2})^2$, or $(d_{5/2} \otimes g_{7/2})$ states. Both restricted basis shell model calculations and pair truncated shell model calculations [8] suggest a significant change in structure between the 6^+ and 4^+ yrast states in ^{136}Ba, which gives rise to a relatively low $B(E2; 6^+ \rightarrow 4^+)$ value in this nucleus [9].

The current paper investigates the yrast states of the $N = 80$ isotone, ^{138}Ce and in particular focuses on the measurement of the yrast $I^\pi = 6^+ \rightarrow 4^+$ reduced transition probability, which is used as a direct comparison for shell model calculations in the region. The decay half-lives for other, yrast excited states of ^{138}Ce have also been established.

II. EXPERIMENTAL DETAILS

The fusion-evaporation reaction ^{130}Te(^{12}C,$4n$) at a beam energy of 56 MeV was used to populate the excited states of ^{138}Ce. The beam was provided by the Tandem van de Graaff accelerator at the National Institute for Physics and Nuclear Engineering, Bucharest, Romania. The target consisted of a 1 mg/cm^2 thick enriched ^{130}Te foil on a 20 mg/cm^2^{208}Pb backing. The experiment was performed using a continuous dc beam over a period of 2.5 days, with an average on-target beam current of approximately 10 pnA. The production cross section for the ^{130}Te(^{12}C,$4n$)^{138}Ce reaction was estimated using the PACE4 code [10] to be ~650 mb. The deexciting γ rays were detected by an array of eight $LaBr_3$(Ce) scintillator detectors and eight high-purity germanium detectors (HPGe) [11]. One of the HPGe detectors had an active Compton suppression shield while the other seven were unsuppressed. The HPGe detectors were placed in three angular rings: five detectors at backward angle ~143° relative to the beam direction, two at ~90°, and one at a forward angle of ~43°. The $LaBr_3$(Ce) detectors were positioned above (three) and below (five) the target chamber at angles of ~45° with respect to the beam direction. The target-detector distance was measured to be ~20 cm for all detectors. Three different sizes of $LaBr_3$(Ce) crystal were used in the present work, having crystal dimensions of (a) (three) 2 × 2 in. cylindrical; (b) (three) 1.5 × 1.5 in. cylindrical and (c) (two) 1 × 1.5 in. conical. Typical full width at half maximum (FWHM) energy resolutions at 1.33 MeV were 2.2–2.8 keV and 30 keV for the HPGe detectors and $LaBr_3$(Ce) detectors, respectively [12].

Data were collected in triple coincidence mode, such that (i) Ge-Ge-Ge or (ii) $LaBr_3$(Ce)-$LaBr_3$(Ce)-Ge γ-ray energy coincidences were measured. The coincidence master gate time window was $\sim$50 ns. A total of $\sim 4\times10^8$ $LaBr_3$(Ce)-$LaBr_3$(Ce)-Ge coincidences were recorded during the experiment for subsequent offline analysis.

III. DATA ANALYSIS

The data were sorted offline into a range of γ-ray energy and time difference coincidence matrices and cubes, such as those described in Ref. [11]. These were then interrogated offline using different γ-ray energy conditions and analyzed with the GASPWARE [13] and RADWARE [14] packages. To correct for instrumental drifts of the $LaBr_3$(Ce) detectors, a run-by-run gain matching procedure was applied. Energy and efficiency calibrations for the response of the detectors in the array were performed using standard ^{152}Eu, ^{137}Cs, and ^{60}Co point sources placed at the target position. The instrument time response for each $LaBr_3$(Ce) detector and constant fraction discriminator (CFD) combination in the mixed array required an offline correction for the low-energy time walk. To achieve this, the method described by Mărginean *et al.* [11] was used.

Two-dimensional $LaBr_3$(Ce) (E_γ-E_γ) matrices and $E_{\gamma1}$-$E_{\gamma2}$-ΔT cubes were created during the offline analysis. A 2D matrix (energy vs time difference) was constructed for the HPGe detectors and was used as offline software gating conditions for the $LaBr_3$(Ce) $E_{\gamma1}$-$E_{\gamma2}$-ΔT cubes. The $I^\pi = 10^+$, $T_{1/2}$ = 81(2) ns isomeric state in ^{138}Ce [15] provided discrete reference energy peaks in the 2D matrix. A condition that the $LaBr_3$(Ce) (E_γ-E_γ) coincidence should be anticipated before the signal from the HPGe detectors was used to isolate $LaBr_3$(Ce) (E_γ-E_γ) coincidences associated with transitions below the $I^\pi = 10^+$ isomeric state in ^{138}Ce. $LaBr_3$(Ce) (E_γ-E_γ) coincidence signals arriving after that of the HPGe detectors were similarly used for transitions above the $I^\pi = 10^+$ isomeric state. Figure 1 shows an example of this 2D matrix for one of the HPGe detectors. The software conditions applied to clean the $LaBr_3$(Ce) $E_{\gamma1}$-$E_{\gamma2}$-ΔT cubes are also indicated.

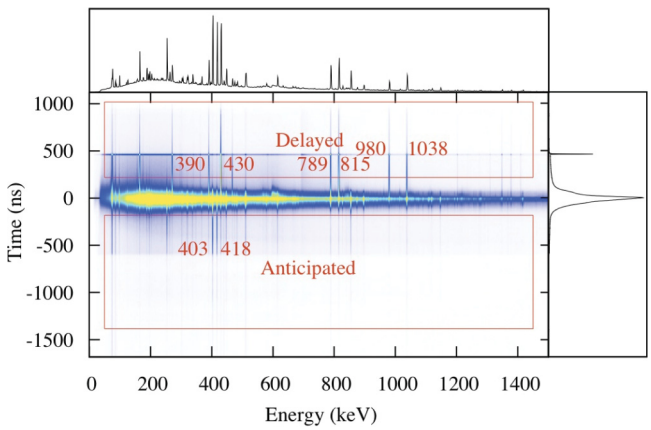

FIG. 1. (Color online) Two-dimensional energy vs time matrix for one of the HPGe detectors. The software gates used to select transitions below and above the $I^\pi = 10^+$ isomeric state are also indicated.

For the half-life measurements, two different techniques were used: (i) the centroid shift method [16,17] and (ii) a fit with a single exponential decay and a prompt response convolution for decays which are significantly longer than the $LaBr_3$(Ce) timing resolution. The centroid shift method, as first introduced by Bay [18], was used in the present work in cases where the lifetime of the nuclear state was significantly shorter than the time resolution (FWHM) for the $LaBr_3$(Ce) coincidences.

IV. RESULTS

The partial level scheme of ^{138}Ce deduced in the current work is shown in Fig. 2. This is consistent with that reported by Bhattacharjee *et al.* [19]. Relative γ-ray intensities have been measured and normalized with respect to the 789 keV ($2^+ \rightarrow 0^+$) transition. The total projection spectra of the E_γ-E_γ coincidence matrices from the ^{130}Te + ^{12}C fusion-evaporation reaction are shown in Fig. 3(a) where the black line is the total projection from HPGe detectors and the red (gray) line is the equivalent spectrum from the $LaBr_3$(Ce) detectors. Figure 3(b) shows the total projection from the

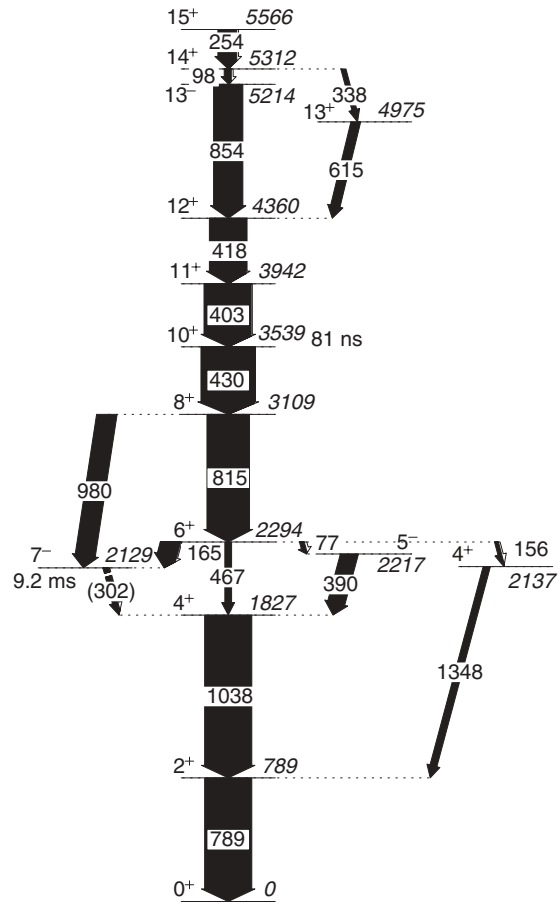

FIG. 2. Partial level scheme of ^{138}Ce observed in the present work. The widths of the arrows connecting the levels are proportional to the γ-ray intensities.

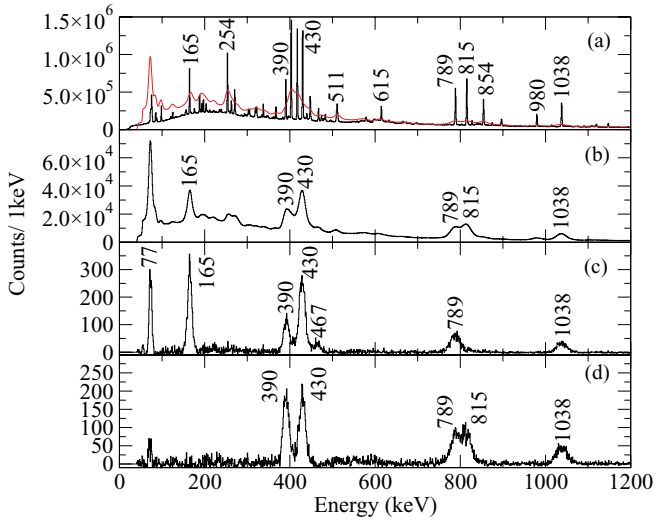

FIG. 3. (Color online) (a) Total projection for all HPGe and $LaBr_3$(Ce) detectors. (b) Total projection for all $LaBr_3$(Ce) detectors with "anticipated" HPGe timing gate. (c) and (d) γ-ray spectra obtained by gating with the 815 and 77 keV transitions in the symmetric $LaBr_3$(Ce) (E_γ-E_γ) coincidence energy matrix with the anticipated HPGe timing gate.

$LaBr_3$(Ce) detectors (E_γ-E_γ) matrix with an anticipated HPGe timing gate for transitions below the $I^\pi = 10^+$ isomer. The energy spectra shown in Figs. 3(c) and 3(d) were obtained by gating with the 815 and 77 keV transitions on the symmetric $LaBr_3$(Ce) (E_γ-E_γ) coincidence energy matrix, respectively, with an anticipated HPGe timing gate.

Figure 4 shows the half-life measurements obtained using the centroid shift method by gating on feeding and deexciting transitions across levels of interest in the sorted $E_{\gamma 1}$-$E_{\gamma 2}$-ΔT cubes with additional timing conditions in the HPGe selecting γ rays below or above the $I^\pi = 10^+$ isomer in ^{138}Ce.

Figure 4(a) presents the time spectra associated with the decay of the yrast $I^\pi = 5^-$ state in ^{138}Ce. An extracted experimental half-life of $T_{1/2} = 450(30)$ ps was obtained from the centroid shift of the time distribution of (77, 390) (black line) and (390, 77) (red line) gates in the $LaBr_3$(Ce) detectors. Figure 4(b) shows the time spectra of the $I^\pi = 11^+$ yrast state which give a value of $T_{1/2} = 140(11)$ ps obtained from the centroid shift of the time distribution associated with the (418, 403) and (403, 418) coincident transitions. Figure 4(c) shows the extracted half-life for the decay of the yrast $I^\pi = 14^+$ state. A measured half-life of $T_{1/2} = 80(9)$ ps was obtained using the centroid shift for the two difference distributions gated on the (254, 338) and (338, 254) transitions. Figure 4(d) corresponds to a prompt coincidence between the (1038, 789) and (789, 1038) pair and shows no measurable shift. The $I^\pi = 2^+$ state half-life was measured previously to be 2.06(14) ps [20]. The FWHM time resolution of 460(10) ps was obtained by a Gaussian fit for the (1038, 789) coincidence. Figures 4(e) and 4(f) show the time distributions associated with the $I^\pi = 4^+$ and 8^+ yrast states. No measurable shift was observed, which indicates that the half-lives for the $I^\pi = 4^+$ and 8^+ yrast states are shorter than 50 ps.

Figure 5 shows the measurement of the half-life of the yrast $I^\pi = 6^+$ state, resulting from the time differences between (a) 815 and 467, (b) 815 and 165, and (c) 815 and 165 keV. The time difference spectra in Figs. 5(a) and 5(b) were fitted with an exponential decay convoluted with a Gaussian [FWHM=460(10) ps] and gave values of the half-life of the $I^\pi = 6^+$ state of (a) $T_{1/2} = 860(60)$ ps and (b) $T_{1/2} = 920(25)$ ps, respectively. Figure 5(c) shows the time distributions for the decay of the $I^\pi = 6^+$ state using the centroid shift method. The time distribution, which is plotted as a black line, is obtained with a (815, 165) energy gate, while the symmetric,

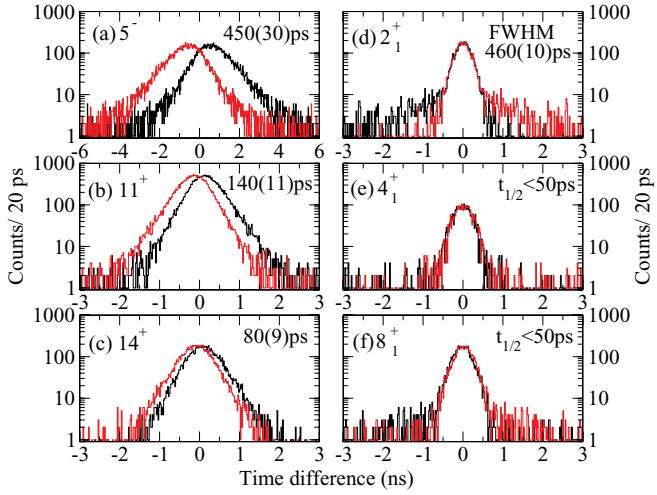

FIG. 4. (Color online) Time difference spectra for yrast states in ^{138}Ce, obtained using the centroid shift method showing the time difference between (a) 77 and 390, (b) 418 and 403, (c) 254 and 338, (d) 1038 and 789, (e) 390 and 1038, and (f) 430 and 815 keV transitions. Time difference spectra plotted with black lines are gated on ($E_{\gamma 1}$, $E_{\gamma 2}$), while the red (gray) lines show the reverse gating.

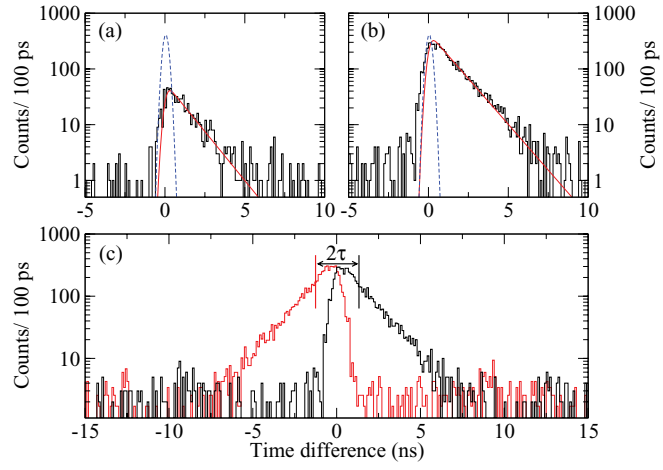

FIG. 5. (Color online) Time spectra obtained in ^{138}Ce from the $LaBr_3$(Ce) $E_{\gamma 1}$-$E_{\gamma 2}$-ΔT cube with an anticipated HPGe gate showing the time difference between (a) 815 and 467 keV, (b) 815 and 165 keV, and (c) (815, 165) and reversed (165, 815) energy gates using the centroid shift method. The continuous lines in (a) and (b) are Gaussian exponential convolution fits to the spectra. The dashed curve is a Gaussian prompt distribution (PRF) with FWHM = 460(10) ps.

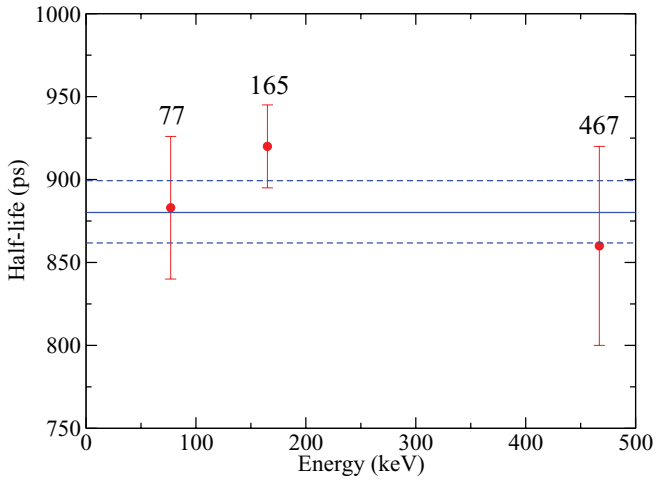

FIG. 6. (Color online) Three measurements of the half-life of the $I^\pi = 6^+$ yrast state from the time difference between 815 keV γ-ray and 77, 165, and 467 keV γ rays. The horizontal solid line indicates the weighted average of the three values and the dashed lines are the uncertainty.

time-reversed (165, 815) gate is plotted in red (gray). The resulting half-life is consistent with that obtained from the exponential decay component. The measured half-lives of the $I^\pi = 6^+$ yrast state are plotted versus the gating γ-ray energy in Fig. 6. The solid line corresponds to the weighted average of these half-lives which has a value of $T_{1/2} = 880(19)$ ps.

V. DISCUSSION

The nucleus $^{138}_{58}Ce_{80}$ has eight valence protons outside the closed $Z = 50$ shell and two neutron holes with respect to $N = 82$. Table I summarizes the decay half-lives obtained from the present work in ^{138}Ce. These are discussed individually below.

A. Half-life of the 6^+ state at 2294 keV

The 2294 keV level has been previously identified in ^{138}Ba(α,4$n\gamma$) studies [21,22] and has a well-established spin and parity of $I^\pi = 6^+$ [23] from angular distribution measurements. The state deexcites to the $I^\pi = 5^-$ state via an $E1$ transition with an energy of 77 keV. It also decays directly to the yrast $I^\pi = 7^-$ state via another $E1$ with a transition energy of 165 keV. A third decay branch from the yrast $I^\pi = 6^+$ state is observed via a 467 keV $E2$ transition to the yrast $I^\pi = 4^+$ state in ^{138}Ce. Also, it decays to the $I^\pi = 4_2^+$ state via an $E2$ transition with an energy of 156 keV (see Fig. 2). Müller *et al.* [24] suggested that the $I^\pi = 6^+$ state consists mainly of a $\pi(d_{5/2} \otimes g_{7/2})$ or $\pi(g_{7/2})^2$ configuration. The extracted half-life from the current work gives a $B(E2) = 0.101(24)$ W.u. for the 467 keV transition, $B(E2) = 9.5(25)$ W.u. for the 156 keV transition, $B(E1) = 3.2(8)\times10^{-5}$ W.u. for the 165 keV transition, and $B(E1) = 1.1(4)\times10^{-4}$ W.u. for the 77 keV transition. $E1$ transitions are typically hindered by a factor of 10^4–10^5 compared to their Weisskopf estimate.

The plot of the systematics of the $B(E2; 6_1^+ \rightarrow 4_1^+)$ values for cerium and barium isotopes, shown in Fig. 7, indicates that the $E2$ transition to the $I^\pi = 4_1^+$ level is more hindered than the corresponding $B(E2)$ value for the $N = 82$, magic nucleus ^{140}Ce.

A similar situation was reported in ^{136}Ba [7] where $B(E2; 6_1^+ \rightarrow 4_1^+) < B(E2; 6_1^+ \rightarrow 4_2^+)$. This was interpreted by assuming that the $I^\pi = 6^+$ and the $I^\pi = 4_2^+$ states have similar configurations dominated by $\pi(g_{7/2})^2$ and $\nu(h_{11/2})^{-2}$ excitations [7].

TABLE I. Transition rates for γ decay from excited states in ^{138}Ce and ^{140}Ce.

Nucleus	E_x (keV)	$J_i^\pi \rightarrow J_f^\pi$	E_γ (keV)	$T_{1/2}$ (ps)	$L\lambda$	Branch (%)*	$B(\lambda L)$ (W.u.)	
							Expt.	SM
^{138}Ce	789	$2^+ \rightarrow 0^+$	789	2.06(14)[a]	$E2$	100	21.2(14)	15.5
	1827	$4^+ \rightarrow 2^+$	1038	<50	$E2$	100	>0.23	21.2
	2217	$5^- \rightarrow 4^+$	390	450(30)	$E1$	78.9	$7.4(8)\times10^{-6}$	[b]
	2294	$6^+ \rightarrow 4^+$	467	880(19)	$E2$	15	0.101(24)	0.967
	2294	$6^+ \rightarrow 4_2^+$	156	880(19)	$E2$	6.5	9.5(25)	0.008
	2294	$6^+ \rightarrow 7^-$	165	880(19)	$E1$	53	$3.2(8)\times10^{-5}$	[b]
	2294	$6^+ \rightarrow 5^-$	77	880(19)	$E1$	25	$1.1(4)\times10^{-4}$	[b]
	3109	$8^+ \rightarrow 6^+$	815	<50	$E2$	70	>0.52	7.5
	3539	$10^+ \rightarrow 8^+$	430	81(2)[a] ns	$E2$	100	0.0110(3)	0.04
	3942	$11^+ \rightarrow 10^+$	403	140(11)	$M1$	93.8	$2.34(19)\times10^{-3}$	[b]
	5312	$14^+ \rightarrow 13^+$	338	80(9)	$M1$	43	$3.1(19)\times10^{-3}$	[b]
	5312	$14^+ \rightarrow 13^-$	98	80(9)	$E1$	57	$1.9(4)\times10^{-3}$	[b]
^{140}Ce	1596	$2^+ \rightarrow 0^+$	1596	0.0916(19)[a]	$E2$	100	13.8(3)	10.9
	2083	$4^+ \rightarrow 2^+$	487	3.45(3)[a] ns	$E2$	100	0.137(4)	1.1
	2108	$6^+ \rightarrow 4^+$	25	7.3(15)[a] μs	$E2$	100	0.29(6)	0.89
	3715	$10^+ \rightarrow 8^+$	202	23.1(4)[a] ns	$E2$	29	0.46(13)	2.08

[a]Taken from Ref. [36].
[b]$E1$ transitions are strictly forbidden in this SM space.

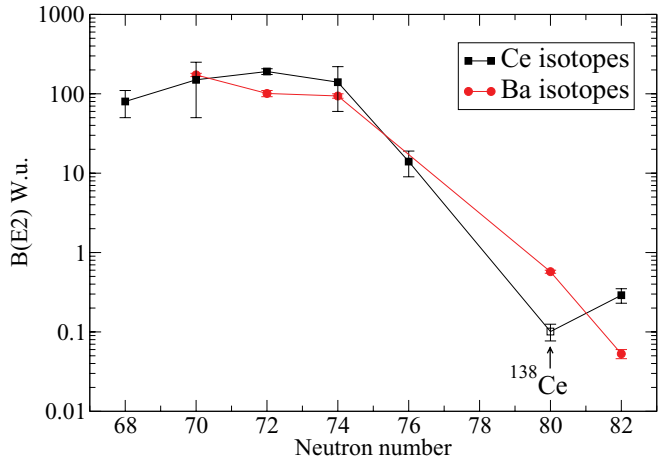

FIG. 7. (Color online) Systematics of $B(E2; 6_1^+ \rightarrow 4_1^+)$ values for cerium and barium isotopes, ^{126}Ce [25], ^{128}Ce [26], ^{130,132,134}Ce [27], ^{140}Ce [28], ^{126}Ba [29], ^{128}Ba [30], ^{130}Ba [31], ^{136}Ba [7], ^{138}Ba [32]. The ^{138}Ce data point is obtained from the current work.

B. Half-life of the 5^- state at 2217 keV

The two low-lying negative parity states (the isomer state $I^\pi = 7^-$ at 2129 keV and $I^\pi = 5^-$ at 2217 keV) shown in Fig. 2 were reported previously by Ludziejewski [22] who suggested that the $I^\pi = 5^-$ state arises from the neutron configuration $(d_{3/2}^{-1} \otimes h_{11/2}^{-1})$ with a $(s_{1/2}^{-1} \otimes h_{11/2}^{-1})$ admixture which decays by $E1$ to the 4^+ state. The extracted $B(E1)$ strength for the $5^- \rightarrow 4^+$ transition is $7.4(8) \times 10^{-6}$ W.u.

C. Half-lives of higher-spin states

Bhattacharjee *et al.* [19] assigned the $I^\pi = 11^+$ yrast state at an excitation energy of 3942 keV to decay by a mixed $(M1 + E2)$ multipolarity transition with an energy of 403 keV based on angular distribution measurements. Since the exact value for the mixing ratio is unknown for this transition, the reduced transition probabilities assuming the limiting values of either pure $M1$ or pure $E2$ have been calculated. A previous study [33] placed a half-life limit on the $I^\pi = 11^+$ state of $T_{1/2} \leqslant 1.5$ ns. The measured half-life of $T_{1/2} = 140(11)$ ps from this work gives $B(M1) = 2.34(19) \times 10^{-3}$ W.u. and $B(E2) = 8.2(7)$ W.u. for this transition.

The $I^\pi = 14^+$ state at an excitation energy of 5312 keV is populated via a $\Delta I = 1$ transition of 254 keV from the $I^\pi = 15^+$ state. This state deexcites to the $I^\pi = 13^+$ state via 338 keV transition. It also decays by a 98 keV transition to the $I^\pi = 13^-$ state. In Ref. [19] the 338 keV transition was assigned to have pure $M1$ character. A half-life of $T_{1/2} = 80(9)$ ps was obtained for the $I^\pi = 14^+$ state using the centroid shift method in the current work (see Fig. 4). The resulting reduced transition strengths for the 338 and 98 keV transitions were calculated to be $B(M1) = 3.1(19) \times 10^{-3}$ W.u. assuming a pure $M1$ multipolarity and $B(E1) = 1.9(4) \times 10^{-3}$ W.u., respectively.

VI. SHELL MODEL CALCULATIONS

Shell model calculations were performed for ^{138}Ce and the closed shell system nucleus ^{140}Ce in the current work.

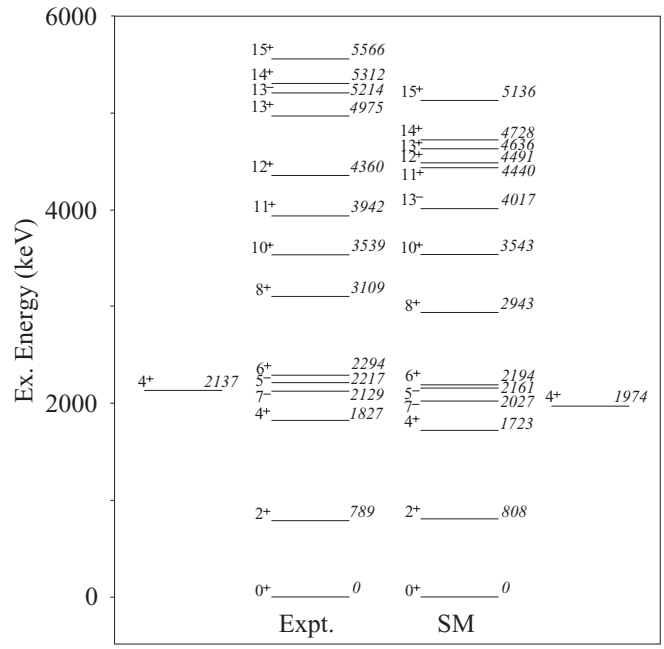

FIG. 8. Comparison of experimental (Expt.) and shell model (SM) energy levels of ^{138}Ce.

These calculations used the NUSHELLX@MSU code [34], with the jj55pn model space and SN100PN interaction [35]. The SN100PN interaction was originally applied to magnetic moments near ^{132}Sn, obtaining good agreement with experiment for the $N = 80$ isotones ^{132}Te and ^{134}Xe. The model space spans $N, Z = 50$–82, comprising the $1g_{7/2}$, $2d_{5/2}$, $2d_{3/2}$, $3s_{1/2}$, and $1h_{11/2}$ orbitals. The proton single-particle energies, taken from states in ^{133}Sb, were -9.68, -8.72, -7.24, -7.34 (estimated) and -6.88 MeV for the $1g_{7/2}$, $2d_{5/2}$, $2d_{3/2}$, $3s_{1/2}$, $1h_{11/2}$ states, respectively. Similarly, the neutron single-hole energies were taken from states in ^{131}Sn, being -9.74, -8.97, -7.31, -7.62, and -7.38 MeV for the $1g_{7/2}$, $2d_{5/2}$, $2d_{3/2}$, $3s_{1/2}$, $1h_{11/2}$ states, respectively. The large number of valence nucleons for ^{138}Ce (eight protons, two neutron holes) necessitates a truncation of the full model space. This was done by forcing the proton $1g_{7/2}$ orbit to contain a minimum of four protons. The remaining four protons and two neutron holes were unconstrained. Calculations for electromagnetic transition rates used the "standard"effective charges of $e_\pi = 1.5e$ and $e_\nu = 0.5e$.

The calculated energy levels of the excited states are compared with experimental data in Fig. 8. At low energies the shell model calculations are in reasonable agreement with the experimental spectrum; the ordering and spacing of levels below the 10^+ state are in good agreement, though states above the yrast 2^+ are typically 100 keV lower than their experimental counterparts. The measured and calculated transition rates are summarized in Table I.

The wave functions for the states of interest are summarized in Table II and found to be strongly mixed, with leading-order partitions typically contributing at the level of ∼10–20%. This will be in part due to the large number of valence nucleons. For the transitions between the first $I^\pi = 6^+$ state and the first and second $I^\pi = 4^+$ states, there is disagreement with experiment.

TABLE II. Shell model wave function compositions for states in ^{138}Ce.

State		Ang. Mom.		π occupancy					ν occupancy					%
I^π	E_x^{Pred} (keV)	π	ν	$g_{7/2}$	$d_{5/2}$	$d_{3/2}$	$s_{1/2}$	$h_{11/2}$	$g_{7/2}$	$d_{5/2}$	$d_{3/2}$	$s_{1/2}$	$h_{11/2}$	
4^+	1723	4^+	0^+	6	2	0	0	0	8	6	2	2	12	7.52
		2^+	2^+	6	2	0	0	0	8	6	3	1	12	4.21
4_2^+	1974	4^+	0^+	6	2	0	0	0	8	6	2	2	12	11.71
				6	2	0	0	0	8	6	4	0	12	5.95
				6	2	0	0	0	8	6	4	2	10	6.50
6^+	2194	6^+	0^+	6	2	0	0	0	8	6	2	2	12	10.98
				6	2	0	0	0	8	6	4	0	12	5.84
				6	2	0	0	0	8	6	4	2	10	4.50
8^+	2943	8^+	0^+	5	3	0	0	0	8	6	2	2	12	9.18
				5	3	0	0	0	8	6	4	2	10	7.35
				5	3	0	0	0	8	6	4	0	12	5.65
10^+	3543	0^+	10^+	6	2	0	0	0	8	6	4	2	10	18.87
		0^+	10^+	4	4	0	0	0	8	6	4	2	10	10.15
		2^+	10^+	6	2	0	0	0	8	6	4	2	10	9.48
		0^+	10^+	4	2	0	0	2	8	6	4	2	10	7.81

The shell model calculations predict the yrast transition is unhindered, with $B(E2; 6^+ \rightarrow 4_1^+) = 0.967$ W.u., whereas the experimentally derived value is 0.101(24) W.u. Conversely, the calculations in this shell model space predict the transition to the second 4_2^+ state is strongly hindered, with $B(E2; 6^+ \rightarrow 4_2^+) = 0.008$ W.u., in contrast to the experimental value of 9.5(25) W.u.

For the corresponding yrast 6^+ to 4^+ transition in ^{140}Ce, a similar, albeit smaller in absolute magnitude, overestimation of the $B(E2)$ is found. Here the experimental transition strength is $B(E2) = 0.29(6)$ W.u., whereas the shell model calculations in the same space as those for ^{138}Ce yield 0.89 W.u. In this case, the second 4^+ is at higher energy than the yrast 6^+, which it does not directly decay to. Since the shell model calculations for $N = 82$ ^{140}Ce only involve valence protons, a calculation in the unrestricted space is possible. A recent study by Srivastava *et al.* [37] using the full jj55pn model space reports a value of 0.15 W.u. for the yrast $6^+ \rightarrow 4^+$ transition in ^{140}Ce, close to the experimental value of 0.29 W.u. This suggests that the truncations applied to the model space in the present work, both for ^{140}Ce and ^{138}Ce, are (at least partially) responsible for the disagreement between the shell model predictions and experimental results for the $B(E2)$ values in these isotopes.

VII. CONCLUSIONS

In summary, the half-life of the $I^\pi = 6^+$ yrast state in ^{138}Ce has been measured to be 880(19) ps which corresponds to a rather hindered transition with $B(E2; 6_1^+ \rightarrow 4_1^+) = 0.101(24)$ W.u. Unusually, the measured $B(E2; 6_1^+ \rightarrow 4_1^+)$ value was found to be less in ^{138}Ce than for the corresponding, neighboring closed shell $N = 82$ isotope ^{140}Ce. The half-lives of the yrast $I^\pi = 5^-$, 11^+, and 14^+ states have also been determined in this work for the first time, with limits on the corresponding reduced electromagnetic transition decay probabilities.

Truncated basis shell model calculations have been carried out to investigate the makeup wave function and $B(E2)$ decay strength from the $I^\pi = 6^+$ yrast state in ^{138}Ce. Comparison with shell model calculations shows a reasonable agreement with the experimental level scheme.

ACKNOWLEDGMENTS

We thank the staff of the Horia Hulubei National Institute of Physics and Nuclear Engineering (IFIN-HH), R-76900 Bucharest, for their excellent technical support during this experiment. This work is supported by the Science and Technology Facilities Council STFC (UK) and STFC Grant No. EP/D077133/1, Almajmaah University (Saudi Arabia), the Romanian Ministry for Education and Research PN-II-ID-PCE-2011-3-0367(UEFISCDI), the DMU02/1 contract with the Bulgarian Science Fund, the Bulgarian-Romanian partnership Contracts No. BRS-07/23 and No. 460/PNII Module III, and the U.S. DOE under Grants No. DE-FG02-91ER40609 and No. FPA2008-06419-C02-01. S.R. and R.B. acknowledge support from the Engineering and Physical Science Research Council (UK).

[1] B. Fogelberg, K. Heyde, and J. Sau, Nucl. Phys. A **352**, 157 (1981).
[2] J. Genevey, J. A. Pinston, C. Foin, M. Rejmund, R. F. Casten, H. Faust, and S. Oberstedt, Phys. Rev. C **63**, 054315 (2001).
[3] G. Lo Bianco *et al.*, Nucl. Phys. A **470**, 266 (1987).
[4] J. C. Merdinger *et al.*, Nucl. Phys. A **346**, 281 (1980).
[5] M. Lach *et al.*, Z. Phys. A **319**, 235 (1984).
[6] H. A. Roth *et al.*, Eur. Phys. J. A **10**, 275 (2001).
[7] M. Fujioka, T. Miyachi, and H. Adachi, Nucl. Phys. A **95**, 577 (1967).
[8] J. J. Valiente-Dobon *et al.*, Phys. Rev. C **69**, 024316 (2004).
[9] A. A. Sonzogni, Nucl. Data Sheets **95**, 837 (2002).

[10] O. B. Tarasov and D. Bazin, Nucl. Instrum. Methods Phys. Res., Sect. B **204**, 174 (2003).
[11] N. Mărginean *et al.*, Eur. Phys. J. A **46**, 329 (2010).
[12] T. Alharbi *et al.*, Applied Radiat. Isot. **70**, 1337 (2012).
[13] D. Bazzacco and N. Mărginean (private communication).
[14] D. Radford, Nucl. Instrum. Methods Phys. Res., Sect. A **361**, 297 (1995).
[15] A. A. Sonzogni, Nucl. Data Sheets **98**, 515 (2003).
[16] H. Mach, R. L. Gill, and M. Moszyński, Nucl. Instrum. Methods Phys. Res., Sect. A **280**, 49 (1989).
[17] J.-M. Regis, G. Pascovici, J. Jolie, and M. Rudigier, Nucl. Instrum. Methods Phys. Res., Sect. A **622**, 83 (2010).
[18] Z. Bay, Phys. Rev. **77**, 419 (1949).
[19] T. Bhattacharjee *et al.*, Nucl. Phys. A **825**, 16 (2009).
[20] G. Lo Bianco, K. P. Schmittgen, K. O. Zell, and P. v. Brentano, Z. Phys. A **332**, 103 (1989).
[21] J. Ludziejewski, P. Koldewijn, and H. Arnold, Nucl. Phys. A **184**, 473 (1972).
[22] J. Ludziejewski and H. Arnold, Z. Phys. A **277**, 357 (1976).
[23] G. Lo Bianco *et al.*, Z. Phys. A **318**, 195 (1984).
[24] M. Müller *et al.*, Nucl. Phys. A **304**, 1 (1978).
[25] T. Ishii, M. Ishii, K. Yanagida and M. Ogawa, Japan Atomic Energy Research Institute Tandem Linac VDG, Annual Report, 1987 (unpublished).
[26] J. C. Wells *et al.*, Phys. Rev. C **30**, 1532 (1984).
[27] D. Husar, S. J. Mills, H. Gräf, D. Pelte, and G. Seiler-Clark, Nucl. Phys. A **292**, 267 (1977).
[28] H. Krehbiel, Phys. Lett. **13**, 65 (1964).
[29] A. Dewald *et al.*, Phys. Rev. C **54**, R2119 (1996).
[30] P. Petkov *et al.*, Phys. Rev. C **62**, 014314 (2000).
[31] O. Stuch *et al.*, Phys. Rev. C **61**, 044325 (2000).
[32] A. Kerek and J. Kownacki, Nucl. Phys. A **206**, 245 (1973).
[33] J. Ludziejewski *et al.*, Phys. Scr. **14**, 133 (1976).
[34] B. A. Brown and W. D. M. Rae, E. McDonald, and M. Horoi, NUSHELLX@MSU, http://www.nscl.msu.edu/~brown/resources/resources.html.
[35] B. A. Brown, N. J. Stone, J. R. Stone, I. S. Towner, and M. Hjorth-Jensen, Phys. Rev. C **71**, 044317 (2005).
[36] NNDC data base, http://www.nndc.bnl.gov/ensdf/.
[37] P. C. Srivastava, M. J. Ermamatov, and Irving O. Morales, arXiv:1210.5789v1.